molecular pharmaceutics

BRIEF ARTICLE

pubs.acs.org/molecularpharmaceutics

Nitroxide Derivatives for Imaging of Hypercholesterolemia-Induced Kidney Dysfunction and Assessing the Effectiveness of Antilipidemic Drugs

Atsuyuki Tomizawa,[†] George Hadjidekov,[‡] Itsuko Ishii,[†] Rumiana Bakalova,[*,§] Zhivko Zhelev,[§] Ichio Aoki,[§] Tsuneo Saga,[§] and Mitsukazu Kitada[∥]

[†]Graduate School of Pharmaceutical Sciences, Chiba University, 1-8-1 Inohana, Chuo-ku, Chiba 260-8675, Japan

[‡]Medical Faculty, Sofia University "St. Kliment Ohridski", 1 Koziak Str., Sofia 1407, Bulgaria

[§]Molecular Imaging Center, National Institute of Radiological Sciences (NIRS), 4-9-1 Anagawa, Inage, Chiba 263-8555, Japan

[∥]Division of Pharmacy, Chiba University Hospital, 1-8-1 Inohana, Chuo-ku, Chiba, 260-8677, Japan

ABSTRACT:

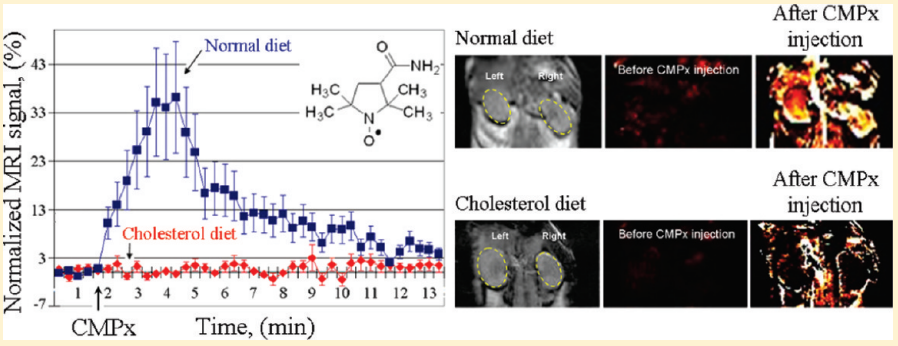

The present study was designed to clarify the possibility for application of nitroxide derivatives in magnetic resonance imaging (MRI) of hypercholesterolemia-mediated renal dysfunction in mice, as well as to assess the effectiveness of antilipidemic drugs (cholestyramine and ezetimibe). The mice were separated in four groups: (i) on a normal diet (ND) without medication (control); (ii) on a high cholesterol diet (CD) without medication; (iii) CD mice receiving cholestyramine; and (iv) CD mice receiving ezetimibe. In CD mice without medication, a hypercholesterolemia was developed, detected by the increasing of total plasma cholesterol and non-HDL cholesterol, and decreasing of HDL cholesterol. The hypercholesterolemia compromised renal function: blood urea nitrogen, creatine and uric acid increased significantly, accompanied with development of glomerulosclerosis, enhancement of the amount of neutrophils and overexpression of metalloproteinase-9. The mice were subjected to anesthesia and MR imaging was performed on 7 T magnet (T1-weighted incoherent gradient-echo sequence; fast low-angle shot). The region-of-interest was selected within the kidney. The images were obtained before and after injection of contrast probe [carbamoyl-PROXYL (CMP) or Gd-DTPA]. In the kidney of ND mice, the MRI signal intensity increased after injection of CMP, reached a maximum (very well-defined renal filtration peak) and decreased to the baseline level within 14 min. In kidney of CD mice, the CMP-mediated enhancement of MRI signal was not detected. Antilipidemic drugs patially abolished the effect of hypercholesterolemia on CMP-enhanced MRI in the kidney. The kinetic curves of Gd-enhanced MRI signal had also different profiles in the kidney of ND and CD mice. They were similar to the profiles of the kinetic curves, obtained from MR urography of healthy human and human with renal pathology, respectively. The present study suggests that CMP is a suitable MRI contrast probe for visualization of hypercholesterolemia-induced renal dysfunction in intact animals and the assessment of the efficacy of antilipidemic drugs. The probe was applied at a concentration that was 3 times lower than the LD50 for intravenous administration in mice. Since the probe is excreted by the kidney, it could be considered harmless for mammalians in the selected dose and appropriate candidate for translational research.

KEYWORDS: nitroxides, ezetimibe, cholestyramine, hypercholesterolemia, renal dysfunction, magnetic resonance imaging

INTRODUCTION

The nitroxide radicals are well-known from electron-paramagnetic resonance (EPR) studies.[1−3] In 1984, it was reported that nitroxide radicals possess comparatively high T_1 contrast properties and could be also applied in magnetic resonance imaging (MRI).[4−6] The nitroxides are small molecules, sensitive to the reduction status of biological samples, and their use in life science research is limited predominantly to tissue redox mapping *in vitro* and *in vivo*, using EPR imaging (EPRI) or MRI.[7−12] The paramagnetic nitroxide radical could be reduced to diamagnetic hydroxylamine with a loss of EPR signal or ^{1}H-MRI

Received: February 23, 2011
Accepted: July 11, 2011
Revised: June 24, 2011
Published: July 11, 2011

dx.doi.org/10.1021/mp200087v | *Mol. Pharmaceutics* 2011, 8, 1962–1969

Scheme 1. Mechanisms of Lowering Plasma Cholesterol by Cholestyramine and Ezetimibe

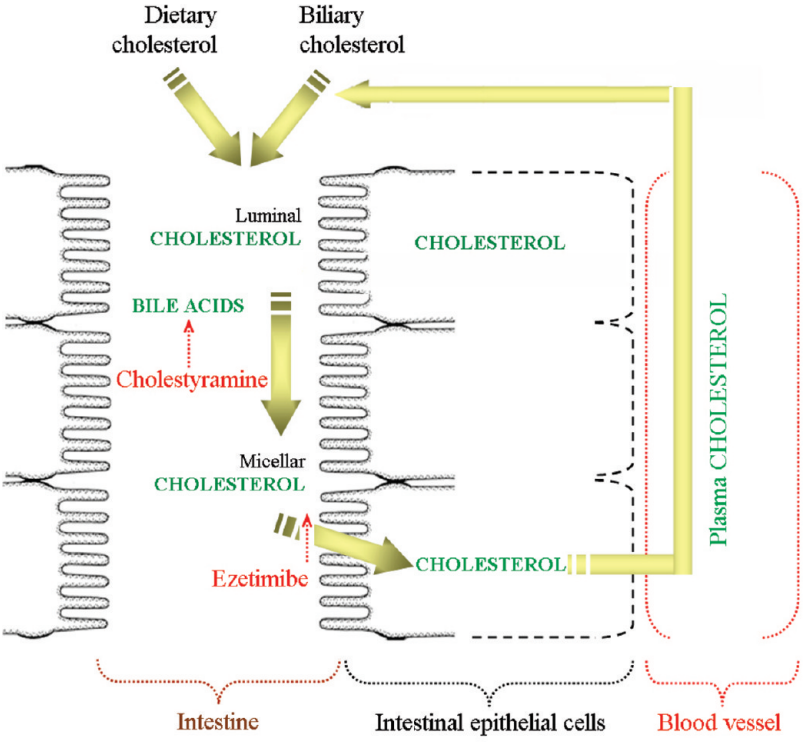

relaxivity and thus to serve as a reduction sensor. However, the diamagnetic hydroxylamine could be reconverted via oxygenation to paramagnetic nitroxide radical with an appearance of EPR signal or ^{1}H-MRI relaxivity and thus to serve as an oxidation sensor. The rate constants of both processes could be used for the evaluation of tissue redox status.

Most MRI studies have employed pyrolidine-type (PROXYL-type) nitroxide radicals due to their higher stability to reduction *in vivo* in comparison with piperidine-type (TEMPO-type) nitroxide radicals.[13−16] The PROXYL-enhanced MRI signal has higher stability and intensity than TEMPO-enhanced MRI signal.[9,13−17] This allows the application of PROXYL derivatives for MR imaging *in vivo* in harmless (low toxic) doses.

It has been reported that water-soluble PROXYL derivatives, e.g. carboxy-PROXYL and carbamoyl-PROXYL, are excreted by the kidney. Since redox status of the kidney varies significantly in dysfunction,[8,18,19] oxidative injury in renal disease is a premise for nitroxide efficiency in evaluating of this pathology. Therefore, PROXYL derivatives can be used as molecular sensors for imaging of renal injury, accompanied by dysbalance of tissue redox activity. The present study was designed to clarify this assumption.

We used carbamoyl-PROXYL as ^{1}H-MRI contrast agent to detect kidney dysfunction in C57Bl/6 mice. Mice with hypercholesterolemia were used as an experimental model. A variety of experimental studies and clinical trials have demonstrated that hypercholesterolemia is a risk factor for the development of chronic kidney disease, accompanied with decreased renal filtration.[20−23]

Our study also aimed to assess the effectiveness of antilipidemic drugs (e.g., cholestyramine and ezetimibe) on renal function in intact animals, using water-soluble PROXYL derivatives and MRI. The mechanisms of antilipidemic effect of cholestyramine and ezetimibe are shown in Scheme 1. Cholestyramine is an ion-exchanged polymer and a bile acid sequestrant. Bile acids are synthesized in the liver from cholesterol and secreted to the intestine through the gallbladder. Cholestyramine binds bile acids in gastrointestinal tract and prevents their reabsorption. The low level of bile acids in the portal vein and liver induces a synthesis of bile acids in the liver and the transport of cholesterol from the plasma. Thus, plasma cholesterol decreases. Ezetimibe is a cholesterol-transport inhibitor. It suppresses cholesterol absorption in the intestine and decreases the plasma cholesterol level.

Studies over the past decade have linked aberrant metalloproteinase (MMP) expression, especially MMP-2 and MMP-9, to a number of renal pathophysiologies.[24] MMP-2 (72 kDa type IV collagenase or gelatinase A) and MMP-9 (92 kDa type IV collagenase or gelatinase B) belong to the subclass of gelatinase. They degrade the components of extracellular matrix in the basal lamina, including collagen, laminin, and zona occludens-1 (ZO-1) in the endothelial tight junctions.[24,25] There is no study that focuses on the cause-end-effect relationship between altered MMP-2 and MMP-9 activity in the plasma and hypercholesterolemia-induced renal dysfunction. Our efforts were directed to estimate the role of both metalloproteinases in this process.

EXPERIMENTAL METHODS

Animals. The care, maintenance, and experiments with animals were in accordance to the "Principles of Laboratory Animal

Table 1. Plasma Cholesterol Levels in Mice on ND or CD with or without Cholestyramine or Ezetimibe[a]

parameter	ND without medication (group 1; $n = 7$)	CD without medication (group 2; $n = 7$)	CD + cholestyramine (group 3; $n = 7$)	CD + ezetimibe (group 4; $n = 7$)
total cholesterol, (mg/dL)	109 ± 3 ref value	288 ± 11 ***	133 ± 5 ns/+++	99 ± 3 ns/+++
HDL cholesterol, (mg/dL)	96 ± 1 ref value	58 ± 5 ***	128 ± 6 ***/+++	75 ± 2 **/+
non-HDL cholesterol, (mg/dL)	13 ± 3 ref value	230 ± 8 ***	5 ± 3 ns/+++	24 ± 3 ns/+++

[a] The results are mean ± SE; ns, non-significant; *** $P < 0.001$, ** $P < 0.01$, * $P < 0.05$ versus group 1 (ND without medication); +++ $P < 0.001$, ++ $P < 0.01$, + $P < 0.05$ versus group 2 (CD without medication); n, number of mice in each experimental group. Group 3 (CD with cholestyramine) versus group 4 (CD with ezetimibe): total cholesterol, nonsignificant; HDL cholesterol, $p < 0.001$; non-HDL cholesterol, $p < 0.05$. All CD mice had significantly elevated serum cholesterol. CD mice in the group receiving cholestyramine and the group receiving ezetimibe had significantly higher HDL cholesterol than ND mice and CD only mice; other cholesterol parameters were significantly lower than those for CD only mice and not different from those for ND mice.

Care" (NIH publication number 85-23, revised 1985) and the Guidelines of the Animal Investigation Committee of Chiba University (Chiba, Japan) and National Institute of Radiological Sciences (Chiba, Japan). Our study protocol was approved by the Animal Care and Use Committee of Chiba University.

Male C57Bl/6 mice were purchased from Charles River Laboratories Japan Inc. (Kanagawa, Japan). Mice were subjected to a normal diet (ND mice) (MF; Oriental Yeast Co., Tokyo, Japan) or a cholesterol diet (CD mice) (ATT6492210; 1.25% [wt/wt] cholesterol, Oriental Yeast Co.), starting at 5 weeks of age. CD mice were separated into three groups: (i) on a CD diet; (ii) on a CD diet, containing 3% cholestyramine; (iii) on a CD diet, containing 0.01% ezetimibe.

Throughout the experiments, the mice were kept in stainless steel cages with food and water available *ad libitum*, and maintained on a 12 h light−dark cycle. At the time of MRI measurements, the mice were between 15 and 17 weeks of age. At the time of all other measurements, the mice were 15 weeks of age.

MRI Measurements on Experimental Animals. The MRI measurements were performed on a 7.0 T horizontal magnet (Kobelco and Jastec, Kobe, Japan) interfaced to a Bruker Avance-I console (Bruker BioSpin, Rheinstetten, Germany) and controlled with ParaVision 4.0.1 (Bruker BioSpin).

Mice were anesthetized by isoflurane (1.2%, Abbott Japan, Tokyo, Japan) and placed in a body holder (Rapid Biomedical, Rimpar, Germany), stomach side down and fixed head. A polyethylene catheter (PE-10, Becton-Dickinson, NJ, USA) was placed in the tail vein for probe administration. The mouse was then placed in the ^{1}H-volume radio frequency (rf) resonator (Bruker BioSpin) with surface rf receiver (Rapid Biomedical). Rectal temperature of the mouse was maintained at 37.0 ± 0.5 °C using an automatic controlled electric heater and monitored using an optical temperature probe (FOT-M and FTI-10, FISO Technology, Quebec, Canada). A respiration sensor (SA Instruments, Edison, NY, USA) was placed on the chest of the mouse for monitoring.

Before probe administration, five control images of the mouse body were acquired with the following parameters: T_1-weighted incoherent gradient-echo sequence (fast low-angle shot); repetition time = 75 ms; echo time = 3.2 ms; flip angle = 45 degrees; number of averages = 4; scan time = 19.2 s; matrix = 64 × 64; slice thickness = 1.0 mm; number of slices = 4. We selected the coronal slice orientations with a 300 × 300 × 1000 μm^3 nominal voxel resolution. Ninety-six seconds after starting the MRI scan (5 images acquired as preadministration data), 100 μL of carbamoyl-PROXYL (Sigma-Aldrich, St. Louis, MO, USA; initial concentration 100 mmol/L, in PBS, pH 7.4) or Gd-DTPA (Meglumine Gadopentetate, Bayer HealthCare, Osaka, Japan; final concentration 0.125 mmol/kg) was injected via the tail vein. T_1-weighted images were acquired continuously within ∼20 min. The MRI data were analyzed using ImageJ (National Institute of Health, Bethesda, MD, USA) software. The MRI signal intensity in the kidney area (region-of-interest) after the injection of nitroxide was normalized to the average MRI signal intensity in the same area before the injection (first 5 frames).

Determination of Plasma Cholesterol Levels. Blood samples were taken from the tail vein in a heparinized microhematocrit tube. The blood samples were centrifuged at 12000*g* for 5 min at room temperature to obtain plasma. Plasma was stored at −80 °C until cholesterol and MMP determination. The total cholesterol levels were determined by a modification of the cholesterol oxidase method with the use of kit reagents (Wako Pure Chemical Industries, Osaka, Japan). The high density lipoprotein (HDL) cholesterol levels were measured by the cholesterol oxidase assay of the supernatant from the precipitate of non-HDL lipoproteins with phosphotungstic acid and magnesium chloride using the kit reagents (Wako Pure Chemical Industries). The non-HDL cholesterol levels were calculated as HDL cholesterol levels subtracted from the total cholesterol levels.

Determination of Plasma MMP-2 and MMP-9 Levels. Enzyme-linked immunosorbent assay (ELISA) was used to determine plasma total MMP-2 and total MMP-9 levels according to the manufacturer's instructions. The MMP-2 ELISA kit (human/mouse/rat MMP-2 [total], Quantikine; R&D Systems, Inc., Minneapolis, MN, USA) detects pro-, active, and tissue inhibitor of metalloproteinase (TIMP)-complexed MMP-2. The MMP-9 ELISA kit (mouse MMP-9 [total], Quantikine; R&D Systems, Inc.) detects pro-, active, and TIMP-complexed MMP-9. Plasma, obtained from the mice at 15 weeks of age, was analyzed.

White Blood Cell Differential Analysis. Blood samples of mice were taken from the tail vein in an EDTA-treated microhematocrit tube. Blood samples for time course analysis of the change of white blood cells were taken from the vena cava in the anesthetized condition with intraperitoneal injection of sodium pentobarbital (40 mg/kg, Dainippon Sumitomo Pharma Co., Osaka, Japan), and the samples were transferred to an EDTA-treated tube. White blood cell differential analyses were performed by an automated hematology analyzer (Advia 120, Bayer Diagnostics, Tarrytown, NY, USA).

Histological Staining. The kidney was fixed with PBS, containing 4% formaldehyde, overnight. Paraffin-embedded cross sections of fixed tissues were stained with hematoxylin and eosin (Wako, Japan).

Statistical Analysis. The results are expressed as mean ± standard error (SE). Statistical analyses were conducted with SAS System Release 8.2 (SAS Institute Inc., Cary, NC, USA). In

Table 2. Biochemical Test of Serum[a]

parameter	ND without medication (group 1)	CD without medication (group 2)	CD + cholestyramine (group 3)	CD + ezetimibe (group 4)
total protein (g/dL)	5.00 ± 0.19 ref value	4.48 ± 0.26 ns	4.88 ± 0.39 ns/NS	4.24 ± 0.05 ns/NS
albumin (g/dL)	3.18 ± 0.15 ref value	2.24 ± 0.05 **	3.16 ± 0.35 ns/+	2.64 ± 0.05 */NS
BUN (mg/dL)	22.62 ± 2.16 ref value	28.05 ± 5.15 *	24.10 ± 3.00 ns/NS	28.86 ± 2.15 ns/NS
CRE (mg/dL)	0.18 ± 0.02 ref value	0.23 ± 0.01 **	0.21 ± 0.08 */NS	0.24 ± 0.01 **/NS
UA (mg/dL)	1.60 ± 0.20 ref value	2.48 ± 0.22 *	2.38 ± 1.53 */NS	2.92 ± 0.86 */NS
Na (mEq/L)	154.00 ± 1.00 ref value	153.75 ± 0.96 ns	152.00 ± 1.22 ns/NS	153.60 ± 0.55 ns/NS
K (mEq/L)	4.76 ± 0.53 ref value	5.48 ± 0.26 ns	6.10 ± 1.29 ns/NS	5.80 ± 0.82 ns/NS
Cl (mEq/L)	112.00 ± 1.58 ref value	111.75 ± 1.50 ns	111.40 ± 0.89 ns/NS	113.00 ± 2.83 ns/NS
Ca (mg/dL)	8.72 ± 0.19 ref value	9.33 ± 0.36 ns	8.60 ± 0.20 ns/NS	9.10 ± 0.38 ns/NS
IP (mg/dL)	8.80 ± 1.55 ref value	7.78 ± 2.15 ns	10.48 ± 1.40 ns/NS	10.22 ± 2.14 ns/NS

[a] BUN, blood urea nitrogen; CRE, creatine; UA, uric acid; IP, inorganic phosphorus. The data was measured by Oriental Yeast Co., Tokyo. The results are mean ± SE; ns, nonsignificant; ** $P < 0.01$, * $P < 0.05$ versus group 1 (ND without medication); NS, nonsignificant; + $P < 0.05$ versus group 2 (CD without medication); *n*, number of mice in each experimental group.

Table 3. Plasma Matrix Metalloproteinases and Neutrophils in Mice on ND and CD with or without Medication[a]

parameter	ND without medication (group 1; $n = 7$)	CD without medication (group 2; $n = 7$)	CD + cholestyramine (group 3; $n = 7$)	CD + ezetimibe (group 4; $n = 7$)
MMP-2, (ng/mL)	218 ± 8 ref value	226 ± 8 Ns	233 ± 6 ns/NS	237 ± 8 ns/NS
MMP-9, (ng/mL)	88 ± 11 ref value	217 ± 21 ***	152 ± 17 ns/+	144 ± 18 ns/+
neutrophils, (%)	11.5 ± 0.7 ref value	36.0 ± 6.6 ***	14.0 ± 0.7 ns/++	20.9 ± 1.1 ns/+

[a] The results are mean ± SE; ns, nonsignificant; *** $P < 0.001$ versus group 1 (ND without medication); NS, nonsignificant; ++ $P < 0.01$, + $P < 0.05$ versus group 2 (CD without medication); *n*, number of mice in each experimental group. Group 3 (CD with cholestyramine) versus group 4 (CD with ezetimibe): MMP-2, nonsignificant; MMP-9, nonsignificant; neutrophils, nonsignificant.

Tables 1−3, the comparisons between the groups were performed with Tukey's multiple comparison test. A value of $p < 0.05$ was considered significant.

RESULTS AND DISCUSSION

Carbamoyl-PROXYL as a Contrast Agent for Magnetic Resonance Imaging of Renal Dysfunction: A Comparison with Gd-DTPA. The mice were subjected to a normal diet (ND mice; control group) or a high cholesterol diet (CD mice), starting at 5 weeks of age. After 15 weeks of age, the mice were used for the analysis. CD mice developed hypercholesterolemia, which resulted in increased levels of total plasma cholesterol and non-HDL cholesterol, and decreased levels of HDL cholesterol (Table 1, group 2 versus group 1).

The hypercholesterolemia compromised the renal function in CD mice: blood urea nitrogen, creatine and uric acid increased significantly. The hystochemical staining shows a development of glomerulosclerosis in CD mice (Figure 1).

The data in Figure 2 represent the dynamics of carbamoyl-PROXYL-enhanced MRI signal in the region-of-interest (ROI; Figure 2A) within the kidney of anesthetized mice. Carbamoyl-PROXYL was applied in a dose of 400 μmol/kg. It is ∼3 times lower than LD50 for its intravenous administration in mice (1.45 mmol/kg). The first five points of the kinetic curve were obtained before the injection of nitroxide (baseline). All data after the injection of nitroxide were normalized to the averaged baseline level. In ND mice, the MRI signal intensity increased after injection of carbamoyl-PROXYL, reached a maximum (renal filtration peak) and then decreased (excretion part) to the baseline level within 14 min (Figure 2B, blue curve). The half-life of MRI signal decay was ∼4 min. In CD mice, the MRI signal intensity after injection of carbamoyl-PROXYL was the same as the baseline, without renal filtration peak and excretion part (Figure 2B, red curve). The color images in Figure 2A show that MRI signal enhancement was not detected in the kidney of CD mice.

There are two possible reasons for this observation: (i) hypercholesterolemia leads to impaired (or reduced) renal filtration, which prevents the penetration of carbamoyl-PROXYL in the kidneys; (ii) hypercholesterolemia leads to a significant increase in reduction potential of the kidneys, which is accompanied with rapid conversion of carbamoyl-PROXYL from radical to hydroxylamine form and loss of MRI signal. The second assumption is unlikely. The previously published data show that hypercholesterolemia induces oxidative stress and inflammatory response, which are involved in renal injury in mammalians.[25−27] All these events are accompanied by an increased level of reactive oxygen species (ROS) and decreased level of endogenous reducing equivalents in the kidneys.[25−27] Therefore, in CD mice, the rate of oxidation of carbamoyl-PROXYL should be considerably higher than the rate of its reduction and loss of T_1 relaxivity should not be observed. Therefore, the absence of nitroxide-enhanced MRI signal in CD mice does not relate to a high redox activity of renal tissue. Presumably, it is a result of fibrosis and significant reduction of renal filtration, triggered by hypercholesterolemia.[25]

Whatever the cause of the kidney dysfunction, the drastic difference between both kinetic curves in Figure 2 shows that carbamoyl-PROXYL is a suitable contrast agent for MR imaging of this anomaly, induced by hypercholesterolemia.

In parallel, we investigated the dynamics of Gd-enhanced MRI signal in the ROI within the kidney of ND and CD mice (Figure 3A1,A2). The kinetic curves had different profiles in

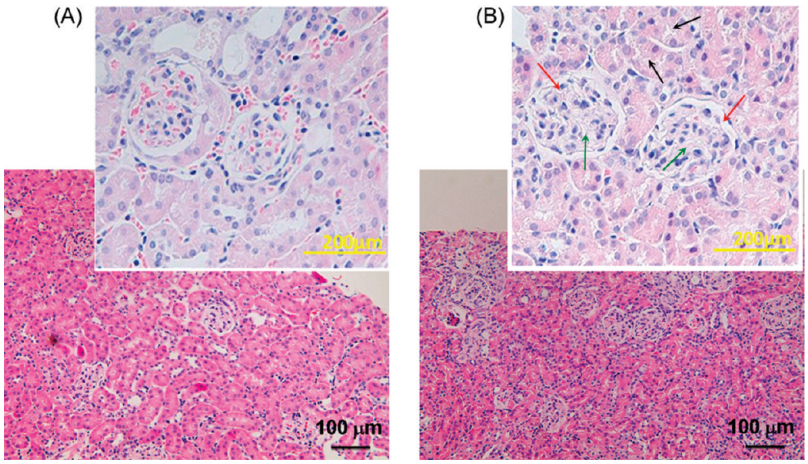

Figure 1. Hematoxylin and eosin staining of tissue sections of kidney, isolated from ND (A) or CD mouse (B). The mice were 15 weeks of age. Red arrow indicates glomerulus with proliferated mesangial cells and reduced blood flow (erythrocytes are not observed). Green arrow indicates initial fibrosis in glomerulus (glomerulosclerosis). Black arrow indicates degeneration of proximal tubules.

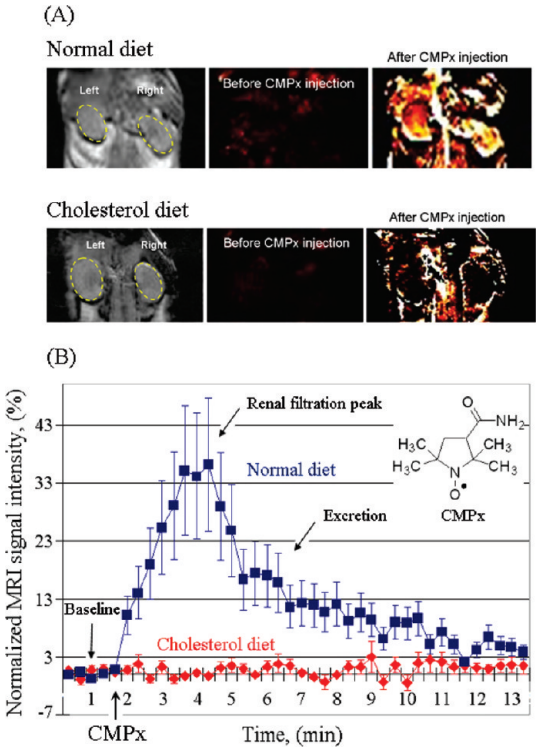

Figure 2. Carbamoyl-PROXYL-enhanced MRI of the kidney in ND and CD mice: Effect of hypercholesterolemia. (A) Black and white images: T_1-weighted MR images of the kidney before the injection of carbamoyl-PROXYL (CMPx). Color images: Extracted MRI signal intensity, normalized to the averaged baseline level (before injection of carbamoyl-PROXYL). (B) Kinetic curves of normalized MRI signal intensity before and after injection of carbamoyl-PROXYL in ND mice (blue curve) and CD mice (red curve). The data are mean ± SE from 5 animals.

comparison with carbamoyl-PROXYL. However, there was also a difference between ND group and CD group. In ND mice, the kinetic curve was characterized with three major parts: (i) baseline (before contrast administration); (ii) renal filtration peak, and (iii) excretion part (Figure 3A1). In CD mice, the renal filtration peak was not well-defined (Figure 3A2). The kinetics of Gd-enhanced MRI signal in the kidney of ND and CD mice was similar to that of humans, subjected to MR urography. Figure 3B represents one typical clinical case. In human, the ROI was placed first around and in the aorta, then around the selected kidney and within the renal parenchyma, excluding the renal pelvis from the analysis. In healthy human, the MRI signal dynamics in this ROI was characterized by four major parts: (i) baseline; (ii) arterial peak; (iii) glomerular filtration peak; and (iv) excretion part (Figure 3B1). Vivier et al. have reported that the "area under the curve", from the arterial peak to the point of equilibrium between filtration and excretion, is representative for the glomerular filtration.[28] Figure 3B1 represents the typical enhancement curves in a normal kidney with very well-defined arterial and glomerular filtration peaks and a large "area under the curve". Figure 3B2 represents typical enhancement curves in a damaged kidney. The arterial peak is missing, glomerular filtration peak is poorly defined and the "area under the curve" is very small.

Carbamoyl-PROXYL for Assessment of the Effects of Antilipidemic Drugs on Renal Dysfunction Using MRI. CD mice were treated with antihypercholesterolemia drugs: cholestyramine or ezetimibe. The data in Table 1 show that CD mice in the group receiving cholestyramine and the group receiving ezetimibe had significantly higher HDL cholesterol than the ND mice and the CD only mice. Total cholesterol and non-HDL cholesterol were significantly lower than CD only mice and were not different from ND mice.

The data in Figure 4 show the ability to assess the effectiveness of antilipidemic drugs on renal function, using carbamoyl-PROXYL-enhanced MRI. In the case of cholestyramine-treated CD mice, the MRI signal intensity in the ROI within the kidney followed the same dynamics as the control ND mice: increase during first two minutes after injection of nitroxide, reaching a maximum and decrease to the baseline level within 14 min (Figure 5B, green curve). The half-life of MRI signal decay was ~4 min 30 s. Cholestyramine partially prevents the negative effects of cholesterol diet on renal function. In the case of ezetimibe-treated CD mice, the MRI signal dynamics in the kidney after injection of nitroxide followed the same profile, but not well-defined as in the case of cholestyramine (Figure 5B, green curve). Sometimes the signal was recorded in one kidney, but not in the other (Figure 5A). Ezetimibe manifested a slight

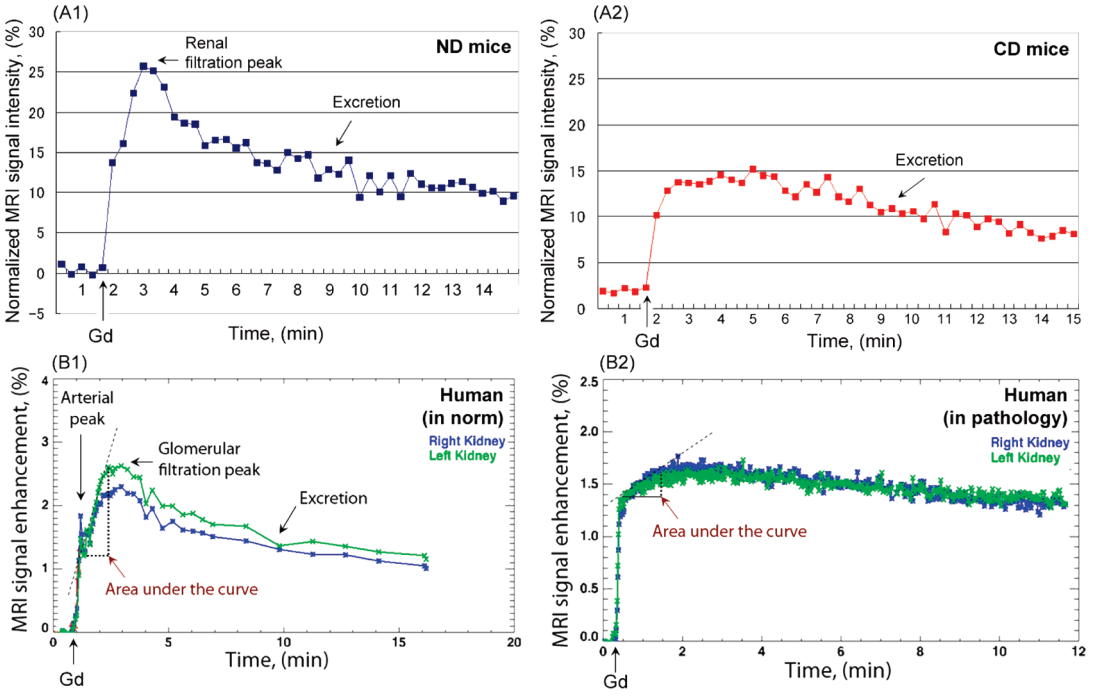

Figure 3. (A) Kinetic curves of normalized MRI signal intensity in kidney before and after injection of Gd-DTPA in ND mice (blue curve) or CD mice (red curve). The data are the mean from 4 animals (SE did not exceed 20%). ImageJ software was used for the data processing. (B) Typical kinetic curves of Gd-enhanced MRI in the ROI within the kidney of healthy human (B1) and human with renal pathology (B2). CHOP-fMRU software was used for the data processing of the postcontrast T_1 VIBE Dynamic sequence in coronal plane during the excretory MR urography.

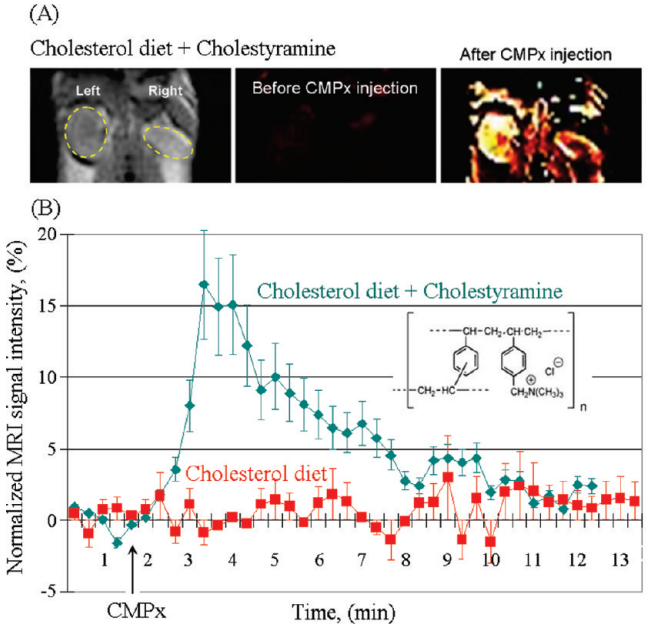

Figure 4. Carbamoyl-PROXYL-enhanced MRI of kidney in CD mice: Effect of cholestyramine. (A) Black and white image: T_1-weighted MR images of the kidney before injection of carbamoyl-PROXYL (CMPx). Color image: Extracted MRI signal intensity, normalized to the averaged baseline level (before injection of carbamoyl-PROXYL). (B) Kinetic curves of the normalized MRI signal intensity before and after injection of carbamoyl-PROXYL in CD mice receiving (red curve) and not receiving cholestyramine (green curve). The data are mean ± SE from 5 animals.

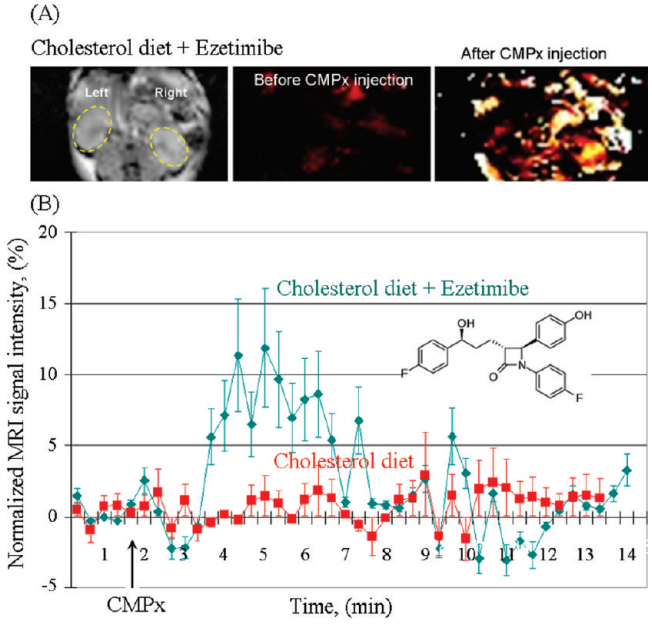

Figure 5. Carbamoyl-PROXYL-enhanced MRI of kidney in CD mice: Effect of ezetimibe. (A) Black and white image: T_1-weighted MR images of kidney before injection of carbamoyl-PROXYL (CMPx). Color image: Extracted MRI signal intensity, normalized to the averaged baseline level (before injection of carbamoyl-PROXYL). (B) Kinetic curves of the normalized MRI signal intensity before and after injection of carbamoyl-PROXYL in CD mice receiving (red curve) and not receiving ezetimibe (green curve). The data are mean ± SE from 5 animals.

positive effect on hypercholesterolemia-mediated renal dysfunction.

The comparative analysis of the results in Figures 4 and 5 shows that the therapeutic efficacy of cholestyramine is better

expressed than that of the ezetimibe and it is possible to assess this efficiency using carbamoyl-PROXYL as MRI contrast agent.

It seems that cholesterol (above some critical level) is a trigger of renal injury. Cholestyramine and ezetimibe reduced the level of total plasma cholesterol to the same degree (Table 1). However, cholestyramine increased the level of HDL cholesterol above the reference value and decreased the level of non-HDL cholesterol below the reference value. In the case of ezetimibe, HDL-cholesterol was 25% below the reference level and non-HDL cholesterol was 2 times above the reference level. It is well-known that HDL fraction is responsible for the transport of the cholesterol in both directions: blood → tissues and tissues → blood. This fraction serves as an antiatherogenic factor. Non-HDL fraction is responsible for transport of the cholesterol in one direction, blood → tissues, and serves as an atherogenic factor. This might be a reason for the better effects observed by cholestyramine on the renal function.

Our study shows that hypercholesterolemia was accompanied by increased plasma levels of MMP-9: three times higher than the reference level (Table 3). The cell fraction, which is responsible for the production of MMP-9, neutrophils, also increased 3 times. This might be one of the mechanisms of kidney damage in CD mice. Cholestyramine and ezetimibe decreased the plasma level of MMP-9 in CD mice, but the values were still about 2 times higher than the reference value. There was a good correlation between the plasma levels of MMP-9 and intensity of carbamoyl-PROXYL-enhanced MRI signal in the kidney area (detected as absolute value of the amplitude of renal filtration peak). In ND mice, the MRI signal enhancement was ∼30%, while in cholestyramine- and ezetimibe-treated CD mice it was ∼17% and ∼10%, respectively.

In conclusion, this study shows that carbamoyl-PROPXYL is a suitable MRI contrast probe for visualization of hypercholesterolemia-induced renal dysfunction and assessment of the efficacy of antilipidemic drugs. The probe was applied in a concentration that was 3 times lower than the LD50 for intravenous administration in C57Bl/6 mice. Since the probe is excreted by the kidney, it could be considered harmless for mammalians in the selected dose.

AUTHOR INFORMATION

Corresponding Author

*Molecular Imaging Center, National Institute of Radiological Sciences (NIRS), 4-9-1 Anagawa, Inage, Chiba 263-8555. Tel: +81-43-206-3274. Fax: +81-43-206-4682. E-mail: bakalova@-nirs.go.jp.

ACKNOWLEDGMENT

We would like to thank Dr. Shigeyoshi Saito and Ms. Sayaka Shibata (Molecular Imaging Center, NIRS-Chiba, Japan) for their technical assistance in the animal experiments on MRI, and Prof. Dr. Antonina Gegova (University hospital "Lozenetz", Sofia, Bulgaria) for the interpretation of the data from histological staining. This work was supported in part by Special Funds (Development of SPECT Probes for Pharmaceutical Innovation) and Grant-in-aid "Kakenhi" from the Ministry of Education, Culture, Sports, Science and Technology, Japan.

ABBREVIATIONS USED

CD, cholesterol diet; carbamoyl-PROXYL (CMPx), 3-carbamoyl-2,2,5,5-tetramethyl-1-pyrrolidineoxy, free radical; EPRI, electron paramagnetic resonance imaging; HDL, high density lipoproteins; LD50, median lethal dose; MMP, matrix metalloproteinase; MRI, magnetic resonance imaging; ND, normal diet; PBS, phosphate buffered saline; TEMPO, 2,2,6,6-tetramethyl-1-piperidinyloxy, free radical

REFERENCES

(1) Rosen, G. M.; Cohen, M. S.; Britigan, B. E.; Pou, S. Application of spin traps to biological systems. *Free Radical Res. Commun.* **1990**, *9*, 187–195.

(2) Valgimigli, L.; Pedulli, G. F.; Paolini, M. Measurement of oxidative stress by EPR radical-probe technique. *Free Radical Biol. Med.* **2001**, *31*, 708–716.

(3) Utsumi, H.; Yamada, K. In vivo electron spin resonance-computed tomography/nitroxyl probe technique for non-invasive analysis of oxidative injuries. *Arch. Biochem. Biophys.* **2003**, *416*, 1–8.

(4) Griffeth, L. K.; Rosen, G. M.; Rauckman, E. J.; Drayer, B. P. Pharmacokinetics of nitroxide NMR contrast agents. *Invest. Radiol.* **1984**, *19*, 553–562.

(5) Afzal, V.; Brasch, R. C.; Nitecki, D. E.; Wolff, S. Nitroxyl spin label contrast enhancers for magnetic resonance imaging. Studies of acute toxicity and mutagenesis. *Invest. Radiol.* **1984**, *19*, 549–552.

(6) Keana, J. F.; Pou, S.; Rosen, G. M. Nitroxides as potential contrast enhancing agents for MRI application: influence of structure on the rate of reduction by rat hepatocytes, whole liver homogenate, subcellular fractions, and ascorbate. *Magn. Reson. Med.* **1987**, *5*, 525–536.

(7) Utsumi, H.; Yamada, K. In vivo electron spin resonance-computed tomography/nitroxyl probe technique for non-invasive analysis of oxidative injuries. *Arch. Biochem. Biophys.* **2003**, *416*, 1–8.

(8) Matsumoto, K.; Hyodo, F.; Matsumoto, A.; Koretsky, A. P.; Sowers, A. L.; Mitchell, J. B.; Krishna, M. C. High-resolution mapping of tumor redox status by MRI using nitroxides as redox-sensitive contrast agents. *Clin. Cancer Res.* **2006**, *12*, 2455–2462.

(9) Hyodo, F.; Matsumoto, K.; Matsumoto, A.; Mitchel, J. B.; Krishna, M. C. Probing the intracellular redox status of tumors with MRI and redox-sensitive contrast agents. *Cancer Res.* **2006**, *66*, 9921–9928.

(10) Soule, B. P.; Hyodo, F.; Matsumoto, K.; Simone, N. L.; Cook, J. A.; Krishna, M. C.; Mitchell, J. B. Therapeutic and clinical applications of nitroxide compounds. *Antioxid. Redox Signaling* **2007**, *9*, 1731–1743.

(11) Zhelev, Z.; Bakalova, R.; Aoki, I.; Matsumoto, K.; Gadjeva, V.; Kanno., I. Nitroxyl radicals for labeling of conventional therapeutics and noninvasive magnetic resonance imaging of their permeability for blood-brain barrier: relationship between structure, blood clearance, and MRI signal dynamics in the brain. *Mol. Pharmaceutics* **2009**, *6*, 504–512.

(12) Zhelev, Z.; Bakalova, R.; Aoki, I.; Gadjeva, V.; Kanno, I. Imaging of cancer by redox-mediated mechanism: a radical diagnostic approach. *Mol. Biosyst.* **2010**, *6*, 2386–2388.

(13) Myiake, M.; Shen, J.; Liu, S.; Shi, H.; Liu, W.; Yuan, Z.; Pritchard, A.; Kao, J. P. Y.; Liu, K. J.; Rosen, G. M. Acetoxymethoxy-carbonyl nitroxides as EPR pro-imaging agents to measure O_2 levels in mouse brain: A pharmacokinetic and pharmacodynamic study. *J. Pharmacol. Exp. Ther.* **2006**, *318*, 1187–1193.

(14) Shen, J.; Liu, S.; Miyake, M.; Liu, W.; Pritchard, A.; Kao, J. P. Y.; Rosen, G. M.; Tong, Y.; Liu, K. J. Use of 3-acetoxymethoxycarbonyl-2,2,5,5-tetramethyl-1-pyrrolidinyloxyl as an EPR oximetry probe: Potential for in vivo measurement of tissue oxygenation in mouse brain. *Magn. Reson. Med.* **2006**, *55*, 1433–1440.

(15) Sano, H.; Naruse, M.; Matsumoto, K.; Oi, T; Utsumi, H. A new nitroxyl-probe with high retention in the brain and its application for brain imaging. *Free Radical Biol. Med.* **2000**, *28*, 959–969.

(16) Anzai, K.; Saito, K.; Takeshita, K.; Takahashi, S.; Miyazaki, H.; Shoji, H.; Lee, M. C.; Masumizu, T.; Ozawa, T. Assessment of ESR-CT imaging by comparison with autoradiography for the distribution of a blood-brain-barrier permeable spin probe, MC-PROXYL, to rodent brain. *Magn. Reson. Imaging* **2003**, *21*, 765–772.

(17) Zhelev, Z.; Matsumoto, K.; Gadjeva, V.; Bakalova, R.; Aoki, I.; Zheleva, A.; Anzai, K. EPR signal reduction kinetic of several nitroxyl

derivatives in blood in vitro and in vivo. *Gen. Physiol. Biophys.* **2009**, *28*, 356–362.

(18) Togashi, H.; Matsuo, T.; Shinzawa, H.; Takeda, Y.; Shao, L.; Oikawa, K.; Kamada, H.; Takahashi, T. Ex vivo measurement of tissue distribution of a nitroxide radical after intravenous injection and its in vivo imaging using a rapid scan ESR-CT system. *Magn. Reson. Imaging* **2000**, *18*, 151–156.

(19) Hirayama, A.; Ueda, A.; Oteki, T.; Nagase, S.; Aoyagi, K.; Koyama, A. In vivo imaging of renal redox status during azelnidipine treatment. *Hypertens. Res.* **2008**, *31*, 1643–1650.

(20) Rodriguez-Porcel, M.; Krier, J. D.; Lerman, A.; Sheedy, P. F.; Romero, J. C.; Napoli, C.; Lerman, L. O. Conbination of hypercholesterolemia and hypertension augments renal function abnormalities. *Hypertension* **2001**, *37*, 774–780.

(21) Chemg, Z. Z.; Patari, A.; Aalto-Setala, K.; Novikov, D.; Schlondorff, D.; Holhofer, H. Hypercholesterolemia is a prerequisite for puromycin inducible damage in mouse kidney. *Kidney Int.* **2003**, *63*, 107–112.

(22) Domrongkitchaiporn, S.; Sritara, P.; Kitiyakara, C.; Stitchantrakul, W.; Krittaphol, V.; Lolekha, P.; Cheepudomwit, S.; Yipintsoi, T. Risk factors for development of decreased kidney function in a Southeast Asian population: A 12-year cohort study. *J. Am. Soc. Nephrol.* **2005**, *16*, 791–799.

(23) Nagata, M.; Ninomiya, T.; Doi, Y.; Yonemoto, K.; Kubo, M.; Hata, J.; Tsuruya, K.; Iiida, M.; Iida, M.; Kiyohara, Y. Trends in the prevalence of chronic kidney disease and its risk factors in a general Japanese population: The Hisayama Study. *Nephrol., Dial., Transplant.* **2010**, *25*, 2557–2564.

(24) Catania, J. M.; Chen, G.; Parrish, A. R. Role of matrix metalloproteinases in renal pathophysiologies. *Am. J. Physiol.* **2007**, *292*, F905–F911.

(25) Eddy, A. A. Intestinal fibrosis in hypercholesterolemic rats: role of oxidation, matrix synthesis, and proteolitic cascades. *Kidney Int.* **1998**, *53*, 1182–1189.

(26) Okamura, D. M.; Pennathur, S.; Pasichnuk, K.; Lopez-Guisa, J. M.; Collins, S.; Febbraio, M.; Heinecke, J.; Eddy, A. A. CD36 regulates oxidative stress and inflammation in hypercholesterolemic CKD. *J. Am. Soc. Nephrol.* **2009**, *20*, 495–505.

(27) Montilla, P.; Espejo, I.; Munoz, M. C.; Bujalance, I.; Munoz-Castaneda, J. R.; Tunes, I. Protective effect of red wine on oxidative stress and antioxidant enzyme activities in the brain and kidney induced by feeding high cholesterol in rats. *Clin. Nutr.* **2006**, *25*, 146–153.

(28) Vivier, P. H.; Dolores, M; Taylor, M.; Dacher, J. N. MR urography in children. Part 2: how to use ImageJ MR urography processing software. *Pediatr. Radiol.* **2010**, *40*(5), 739-746.